11A.3 DATA ASSIMILATION STRATEGIES IN THE PLANETARY BOUNDARY LAYER

Brian P. Reen* and David R. Stauffer
Penn State University, University Park, PA

1. INTRODUCTION

Effectively utilizing surface observations and above-surface observations within the planetary boundary layer (PBL; also known as the atmospheric boundary layer) in numerical weather prediction models can be challenging, and thus such observations may not always be fully used in data assimilation. The high degree of spatial and temporal heterogeneity at the surface and in the PBL contributes to the difficulty in using these observations. However, there are many applications, including triggering convection, air chemistry, and transport and dispersion, for which accurate simulation of within-PBL conditions as well as the depth of the PBL is important. Additionally, surface observations often exist at significantly more locations and times than above-surface observations (e.g., radiosondes).

Nudging, also known as Newtonian relaxation, is a continuous form of data assimilation that adds a term to the model tendency equations at each timestep to gradually assimilate observations based on the difference (the innovation) between observations (observation nudging) or a gridded analysis (analysis nudging) and the model (Stauffer and Seaman 1994). Compared to other popular data assimilation methods, nudging is computationally inexpensive and conceptually simple.

Applying the surface mass field (temperature and water vapor) observations to the lowest model level (LML) can result in significant error due to strong near-surface vertical gradients caused by phenomena such as surface superadiabatic layers and nocturnal inversions (e.g., Stauffer et al. 1991). Methods to account for the vertical separation between surface observations and the LML for temperature include extrapolating potential temperature from the LML to the surface (Ruggiero et al. 1996) or assuming a constant surface-layer friction temperature from the LML to the surface and solving for the surface temperature (Ruggiero et al. 2000). This study investigates calculating the innovation using 2-m diagnostic values from the model.

Since surface air temperature (and water vapor) can be strongly coupled with the underlying land surface, some of the difficulty in assimilating surface mass fields is due to surface properties (e.g., soil temperature and moisture) not being directly and consistently affected by the data assimilation. For example, in some PBL schemes (e.g., the nonlocal first-order closure Blackadar PBL scheme; Zhang and Anthes 1982) slight changes to surface air temperature due to data assimilation may improve surface air temperature but cause a sudden large decrease in model-diagnosed PBL height due to a reversal of sign of surface heat flux (e.g., Stauffer et al. 1991; Ruggiero et al. 2000).

The additional use of surface observations to change land surface properties such as soil temperature may bring the land surface into better balance with the assimilation-affected surface air properties. In a one-dimensional (1D) study using a force-restore model (Deardorff 1978), Alapaty et al. (2001) nudged ground temperature based on the changes that would be made to surface fluxes by surface air temperature and water vapor nudging. Childs et al. (2006) and Alapaty et al. (2008) propose a similar method in a three-dimensional (3D) study using MM5-Noah (Chen and Dudhia 2001) that also nudges soil moisture. Based on Coiffier et al. (1986), Giard and Bazile (2000) and Belair et al. (2003) found the analysis increment from optimal interpolation of surface temperature and applied to land surface temperature. Nudging soil temperature based on surface air temperature innovations is investigated in this study.

In addition to accounting for differences between the LML and the observation level and land surface properties, the depth through which to apply the surface observation must also be determined. Since the PBL is often assumed to be well-mixed during free convective conditions, assimilation may be done throughout the PBL (e.g., Stauffer et al. 1991 with analysis nudging; Benjamin et al. 2004 with 3DVAR). In WRF and MM5 obs nudging, Liu et al. (2005) spread LML innovations using 2-m above-ground-level (AGL) temperature throughout the PBL with weights decreasing with height. Model diffusion (Ruggiero et al. 1996; Gallus and Segal 2001) and vertical correlations of observations (Hacker and Roskier-Edelstein 2007) have also been used to limit the vertical extent of application. This study will investigate vertical influence functions dependent on atmospheric conditions.

Above-surface observations are more routinely assimilated above the PBL or some other level where errors are often correlated over larger spatial and temporal scales than within the PBL (e.g., Stauffer and Seaman 1994; Pleim and Xiu 2003; Schroeder et al. 2006). The issue of smaller temporal scales of correlation within the PBL than in the free atmosphere can be mitigated if data is available more frequently than the standard 12-h radiosondes (Seaman et al. 1995), as with the 3-h radiosondes available for this study.

This paper applies obs nudging (Stauffer and Seaman 1994) in both a 1D and a 3D version of the MM5 to investigate improved methods to assimilate surface (2 m) and above-surface mass-field observations for dynamic initialization (DI) and dynamic

* *Corresponding author address:*
Brian P. Reen, 503 Walker Building, University Park, PA 16802; email: reenb@meteo.psu.edu

analysis (DA). Section 2 describes the model and Section 3 the case studies. The experimental design is presented in Section 4, results are discussed in Section 5, and summary and conclusions are given in Section 6.

2. MODEL DESCRIPTION

The nonhydrostatic Fifth-Generation Pennsylvania State University / National Center for Atmospheric Research (PSU/NCAR) Mesoscale Model (MM5; Dudhia 1993; Grell et al. 1995) is used for this study. A 1D model is used to focus on the first-order effects of the proposed data assimilation techniques and then the 3D model tests the methods that perform best in 1D.

The PSU 1.5-order (level 2.5) TKE-predicting scheme (Stauffer et al. 1999; Shafran et al. 2000), also known as the Gayno-Seaman (GS) scheme is used. The GS scheme diagnoses the PBL top as the height at which TKE decreases below a threshold (0.1 $m^2 s^{-2}$ if maximum TKE in the vertical column is at least 0.2 $m^2 s^{-2}$).

The National Centers for Environmental Prediction—Oregon State University—Air Force—Hydrologic Research Laboratory (Noah) LSM (Ek et al. 2003) is coupled to GS for this study. The Noah LSM provides prognostic equations for canopy water and four-layer soil temperature and soil moisture, and has the potential to more accurately model the surface-air interface than the force-restore slab model (Grell et al. 1995). The Rapid Radiative Transfer Model (RRTM; Mlawer et al. 1997) is used for longwave radiation while the Dudhia (1993) cloud-radiation scheme is used for shortwave. Explicit microphysics including simple ice processes (no mixed phases; Dudhia 1993) is applied without any convective parameterization.

By default the GS scheme uses a background vertical diffusion coefficient of 0.50 $m^2 s^{-1}$ below ~60 m above ground level (AGL) and 0.05 $m^2 s^{-1}$ above ~160 m AGL with a linear transition. This was found to result in excessive vertical mixing and so all experiments use a background vertical diffusion of 0.10 $m^2 s^{-1}$ below ~60 m AGL.

3. CASE DESCRIPTION

The experiments described in the next section were completed during the International H_2O Project (IHOP; Weckwerth et al. 2004; LeMone et al. 2007), a field experiment during May and June of 2002 in the Southern Great Plains region of the United States.

Three IHOP days are studied: 29 May, 6 June, and 7 June 2002. During the daytime period of 29 May, Oklahoma and Kansas are mostly clear or only have limited cloudiness. On 6 June, at 1200 UTC there is a trough centered at 500 hPa east of Oklahoma but high pressure dominates over Oklahoma and Kansas resulting in generally clear conditions with some clouds in southern Oklahoma. At 1200 UTC on 7 June, an area of surface high pressure stretches from the northeast U. S. southwest to Texas. Oklahoma and Kansas are within this region and Kansas is generally clear with fair-weather cumulus in Oklahoma. These days were chosen for this study because of the available observations and the generally fair-weather conditions.

In addition to normal National Weather Service radiosondes, 3-hourly radiosondes are available on these three case days at five sites in the U. S. Department of Energy's Atmospheric Radiation Measurement (ARM) Southern Great Plains (SGP) facility and they are used in the 1D simulations. There are about 350 surface observations available hourly within the 3D model 4-km domain, including an hourly dataset of surface observations from various data sources compiled by the University Corporation for Atmospheric Research (available at http://www.eol.ucar.edu/projects/ihop/dm).

For the 1D simulations PBL height was diagnosed via manual diagnosis for the 3-hourly soundings (Steve Hanna 2007, personal communication). For the 3D simulations PBL height was diagnosed from aircraft lidar (DLR Differential Absorption Lidar, Poberaj et al. 2002; Leandre II, Bruneau et al. 2001) using wavelet edge-detection methods (Davis et al. 2000).

4. EXPERIMENTAL DESIGN

The MM5 is configured here with 62 vertical sigma layers, with the first half-layer at 30 m AGL, 50-m resolution through the lowest 2 km, and the model top at 50 hPa. All model integrations start at 0000 UTC on three days (29 May, 6 June, and 7 June 2002) and run for 24 hours until 0000 UTC the following day in order to simulate the full diurnal cycle.

For the 3D experiments, nested 36- and 12-km domains centered over the Southern Great Plains are used to provide initial and lateral boundary conditions for the 4-km domain that is the focus of the 3D portion of the study (Fig. 1). The initial conditions and lateral boundary conditions for the outermost domain are obtained from Eta Data Assimilation System (EDAS) analyses enhanced by surface and rawinsonde data via a modified successive scan objective analysis method (Benjamin and Seaman 1985). Analysis nudging of this dataset is used only on the outer two domains and only above the PBL to improve initial and lateral boundary conditions provided to the 4-km domain without disturbing the model-predicted PBL.

The 1D experiments were completed at five locations part of the ARM SGP facility: the Central Facility (CF) and Boundary Facilities 1, 4, 5, and 6 (BF1, BF4, BF5, and BF6) in Oklahoma and Kansas. (Fig. 1). The initial conditions are taken from the 4-km domain's initial conditions.

Vegetation fraction from enhanced vegetation index satellite observations is used for Noah. Output from offline Noah runs (forced by observations rather than coupled to an atmospheric model) from the High Resolution Land Data Assimilation System (HRLDAS; Chen et al. 2004; Chen et al. 2007) are used to specify initial canopy water and initial multiple-level soil moisture and soil temperature.

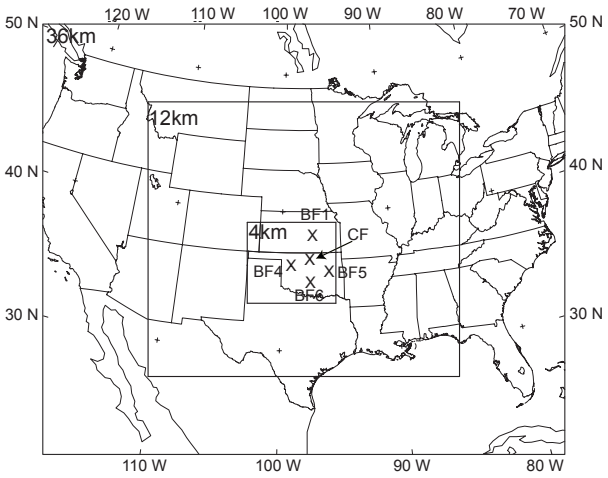

Fig. 1. Locations of the 36-, 12-, and 4-km 3D MM5 domains and the locations of the five 1D simulations at the ARM radiosonde sites (CF, BF1, BF4, BF5, and BF6).

In the standard release version of MM5, above-surface observations are weighted so that they are only applied at a single model level closest to the height of the observation; however surface and within-PBL observations of mass-fields (temperature and water vapor) are not generally assimilated.

MM5 experiments in 1D using DA and DI are used to explore different data assimilation methods, the best of which are then applied in 3D using DI. Details on the 1D DI experiment results are not presented here but may be found in Reen and Stauffer (2009). The 1D DA experiments apply data assimilation throughout the model simulations and demonstrate the maximum benefit realizable via data assimilation; these types of simulations can be used to create an analysis that can then be applied as the meteorology for air quality studies. The 3D DI experiments apply data assimilation up to 1800 UTC, with decreasing weight in the last hour; this methodology can be used in forecasting.

In 1D, the control experiment CTLG does not use any obs nudging (Table 1). Experiment SGA1 adds mass-field surface obs nudging only using the method used in the standard 3D MM5 for wind observations (applied through the lowest 3 layers with weights of 1.00, 0.67, and 0.33 in the lowest three model levels). While in Exp. SGA1, the innovation is calculated by comparing the 2-m observation with the lowest model level (LML) value (~30 AGL), in Exp. SGA2 a 2-m diagnosed model value is used. In Exp. SGA3, the innovations are only applied in the LML, but in Exp. SGA4 during free convective conditions they are applied throughout the PBL. Exp. SGA5 adds soil temperature nudging in the top 10-cm soil layer based on the 2-m air temperature innovation. Using the Noah top soil layer temperature tendency equation (Chen et al. 1996) and the equation for diagnosing 2-m air temperature, one can derive a nudging equation for top soil layer temperature T_1 related to changes in 2-m air temperature T_{2m}:

$$\left.\frac{\partial T_1}{\partial t}\right|_{nud} = \left.\frac{\partial T_{2m}}{\partial t}\right|_{nud}\left(1-\exp\left[-\frac{2K_T}{\Delta z_1^2 C_1}\Delta t\right]\right)$$

where t is time, the "nud" subscript indicates that only the nudging tendencies are being described, K_T is thermal conductivity, Δz_1 is the thickness of the top soil layer, C_1 is the heat capacity of the top soil layer, and Δt is the time over which the change is applied.

In 3D, control experiment CTL again has no obs nudging (Table 2). Exp. DEF uses the default obs nudging configuration which uses wind observations at all levels but mass-field observations only above the PBL. Exp. SFC adds the data assimilation of surface mass-field observations using the methodology in the 1D experiment SGA5. Finally, Exp. SFCBL adds mass-field data within the PBL to the assimilation.

Table 1. Surface obs nudging experimental design. The innovation level indicates the model level compared to the surface observation to compute the innovation, either 2-m values or the lowest model level (LML). The depth of nudging during non-free-convective conditions is either the lowest three layers or only the lowest layer while during free-convective conditions it may be the lowest one layer, three layers, or the entire PBL ("PBL"). Soil T nudging indicates whether the top soil layer's temperature is nudged.

Name	Innov-ation level	Depth of mass-field nudging (layers)		Soil T nudging
		Non-free-convective	Free convective	
CTLG	---	---	---	No
SGA1	LML	3	3	No
SGA2	2 m	3	3	No
SGA3	2 m	1	1	No
SGA4	2 m	1	PBL	No
SGA5	2 m	1	PBL	Yes

Table 2. Experimental design for 4-km 3D MM5 experiments indicating observations utilized and nudging parameter specifications. Note that 2-m temperature and water vapor mixing ratio observations and 10-m and LML wind observations are considered "surface" (Sfc.) and that z_i=PBL top.

Name	Obs Nudging					
	Winds			T / Qv		
	Sfc.	$<z_i$	$>z_i$	Sfc.	$<z_i$	$>z_i$
CTL	No	No	No	No	No	No
DEF	Yes	Yes	Yes	No	No	Yes
SFC	Yes	Yes	Yes	Yes	No	Yes
SFCBL	Yes	Yes	Yes	Yes	Yes	Yes

5. RESULTS

5.1 *1D Experiments*

The mean profiles of air temperature (averaged over the 3 case days and 5 locations) at 0900 UTC (0300 LST) demonstrate the large differences among the experiments overnight (Fig. 2). Note that for model values, the value closest to the surface is a 2-m diagnosed air temperature and other levels are the values at each model level (starting at ~30 m AGL). The observed value plotted closest to the surface is the 2-m surface observation, while other levels are interpolated from the 3-hourly soundings to the model levels. Exp. CTLG shows a pronounced warm bias near the surface for these cases.

The addition of mass-field obs nudging (Exp. SGA1; Fig. 2) significantly cools the near surface air temperature. However, note that at the LML, the model is now significantly cooler than the observation. This is because the innovation was calculated by comparing the 2-m observation with the LML model value (~30 m AGL) meaning that data assimilation is attempting to drag the LML value to the 2-m observation (which is much cooler than the LML observation). Calculating the innovation using the 2-m model-diagnosed value (Exp. SGA2; Fig. 2) ameliorates this issue.

In Exp. SGA2, the top of the surface-based inversion is higher than either the control experiment (Exp. CTLG) or the observations (Fig. 2). Although for these cases, this improves the model air temperature due to the warm bias, in general this may indicate that the influence of the surface is being spread too strongly upward. Limiting the vertical spreading of the innovation to only one level (Exp. SGA3) somewhat improves this. During stable conditions, as seen during the night in these cases, the influence of the surface is limited to near the surface. However, during daytime convective conditions, the influence of the surface should be communicated throughout the well-mixed PBL. To account for this, Exp. SGA4 spreads the innovation from surface observations throughout the PBL. The daytime mean absolute error (MAE) profile (Fig. 3) in the lowest 1000 m AGL improves from 1.2 K for a 1-layer vertical influence to 0.9 K for a 3-layer vertical influence to 0.7 K for a whole-PBL vertical influence.

The temperature of the land-surface does not have time to fully adjust to the changes in the near-surface air temperature, and this results in substantial changes in the vertical profile of temperature in this region (Fig. 4). For example, overnight in the control experiment with no nudging (Exp. CTLG; Fig. 4a) the difference between the top soil layer (10-cm) temperature and the LML air temperature is very small (shaded region). In contrast to this, there is a substantial difference in the experiment using the best methodology found thus far (Exp. SGA4; Fig. 4b). Nudging the top soil layer temperature based on the innovation calculated from the surface temperature restores the balance overnight (Exp. SGA5; Fig. 4c; top soil layer temperature minus LML temperature is 0.1 ˚C for Exp. SGA5, which compares favorably to 0.0 ˚C for Exp. CTLG versus

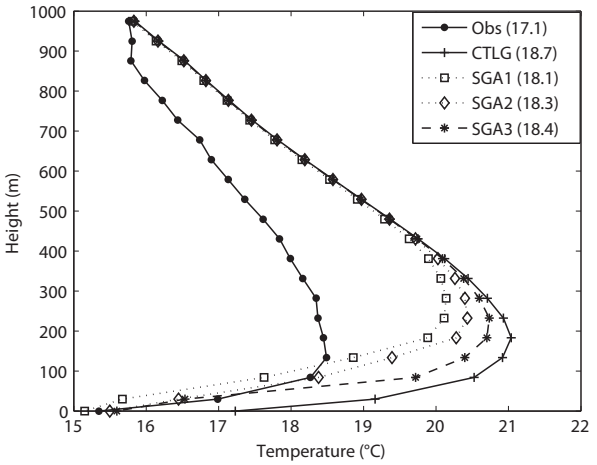

Fig. 2. Temperature profiles (°C, averaged over the five locations and three case days) for observations, the GS control experiment, and selected surface obs nudging DA experiments at 0900 UTC (0300 LST). The lowest point plotted is the 2-m AGL model-diagnosed temperature and the surface temperature observation. Other points plotted are each model level and the radiosonde observations interpolated to this level. The average of each profile is listed in parentheses in the legend.

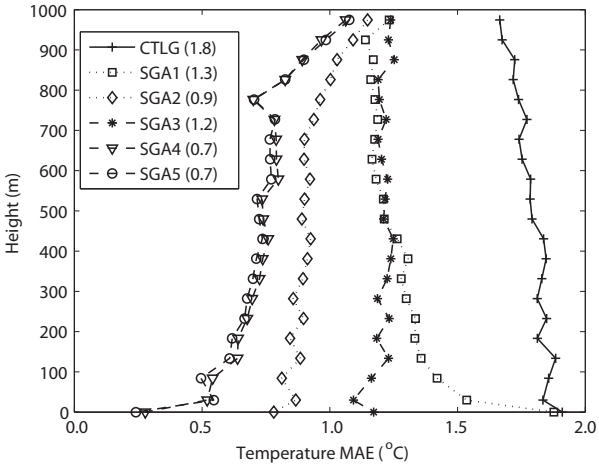

Fig. 3. Temperature MAE profiles (°C, averaged over the five locations and three case days) for observations, the GS control experiment, and selected surface obs nudging DA experiments at 2100 UTC (1500 LST). The average of each profile is listed in parentheses in the legend.

2.2 ˚C for Exp. SGA4). There is also a small improvement in air temperature near the surface overnight (not shown).

The PBL height was found to be degraded by the assimilation of only surface mass-field observations; the MAE for the 1500-0000 UTC period during which diagnoses are available increases from 413 m for Exp. CTLG to 486 m for Exp. SGA5. This is because correction of temperature biases near the surface can

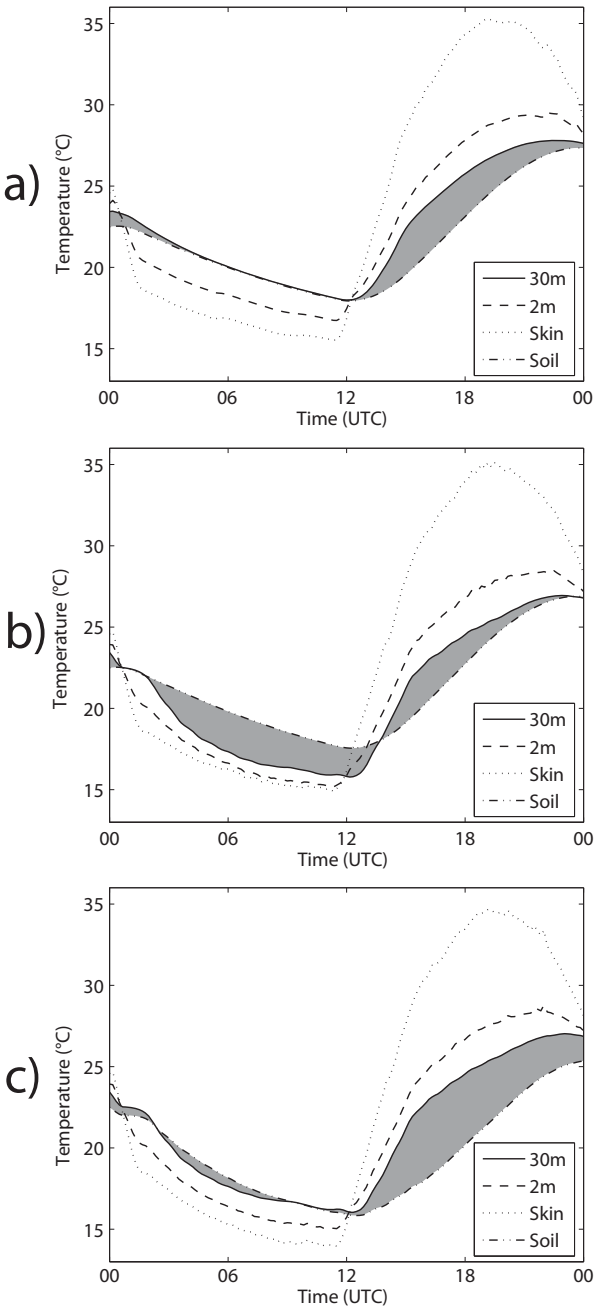

Fig. 4. Time series of lowest model level air temperature (30 m), 2-m temperature, skin temperature, and top layer soil temperature (0-10 cm) (°C, averaged over the five locations and three case days) from 0000 UTC to 0000 UTC the following day (1800 LST to 1800 LST) for a) control experiment CTLG, and DA experiments b) SGA4, and c) SGA5. The difference between LML air temperature and top soil layer temperature is shaded in grey.

change the stabilization of the PBL which is important in determining PBL growth. 1D experiments not shown here indicated that the addition of above-PBL mass-field observations to the data assimilation removes this degradation (MAE 345 m).

5.2 *3D Experiments*

The 3D DI experiments demonstrate the improvements to forecasts due to these data assimilation methods. Fig. 5 shows the temperature MAE for the pre-forecast period (0000 to 1800 UTC) and the forecast period (1900 to 0000 UTC) averaged over the three case days for surface (2 m), 0-150 m, and 150-1000 m layers. In general the inclusion of each additional type of observations in the data assimilation improves the results at each of the three layers.

At 2 m (Fig. 5c) during the DI period (0000-1800 UTC) default nudging (Exp. DEF) improves the results somewhat (MAE from 1.5 to 1.4 K) but more substantial improvements are seen with the addition of surface mass-field observations (Exp. SFC; MAE 0.9 K) and the addition of within-PBL mass-field observations (Exp. SFCBL; MAE 0.9 K). During the forecast period (1900-0000 UTC) Exps. SFC and SFCBL still show a slight improvement over Exp. DEF, and all htree experiments produced lower errors than the FDDA Exp. CTL.

For 0-150 m and 150-1000 m AGL (Fig. 5a-b), the relative importance of surface observations decreases and the relative importance of within-PBL observations increases. By the end of the forecast period the improvement due to surface observations generally is very small, but the use of within-PBL observations still results in a small improvement (~0.1 K).

The model-diagnosed PBL height as compared to the lidar-derived values improves with the use of default data assimilation (Exp. DEF; Table 3) and the addition of surface and within-PBL mass-field observations has little additional effect on PBL height, indicating that observations can be assimilated as proposed in this paper at the surface and within the PBL without adversely affecting PBL heights.

6. SUMMARY AND CONCLUSIONS

Methods to assimilate surface and within-PBL mass-field observations using obs nudging are evaluated using the Noah LSM and the Gayno-Seaman TKE scheme for dynamic analysis (DA) with 1D MM5 simulations and dynamic initialization (DI) with 3D MM5 simulations. These experiments used three case days over the Southern Great Plains during the IHOP field experiment.

Careful assimilation of surface mass-field (temperature and water vapor) observations can improve mesoscale model simulations. To compute the innovation used in assimilation, it is recommended that surface observations be compared to model fields at the height of the observations (2 m AGL), rather than comparing surface observations to lowest model level values (30 m AGL in this study). Due to differences in the vertical mixing and error correlation, the innovation based on the surface observation may be best applied during free convective conditions throughout the PBL, and during other conditions only at the LML. The use of

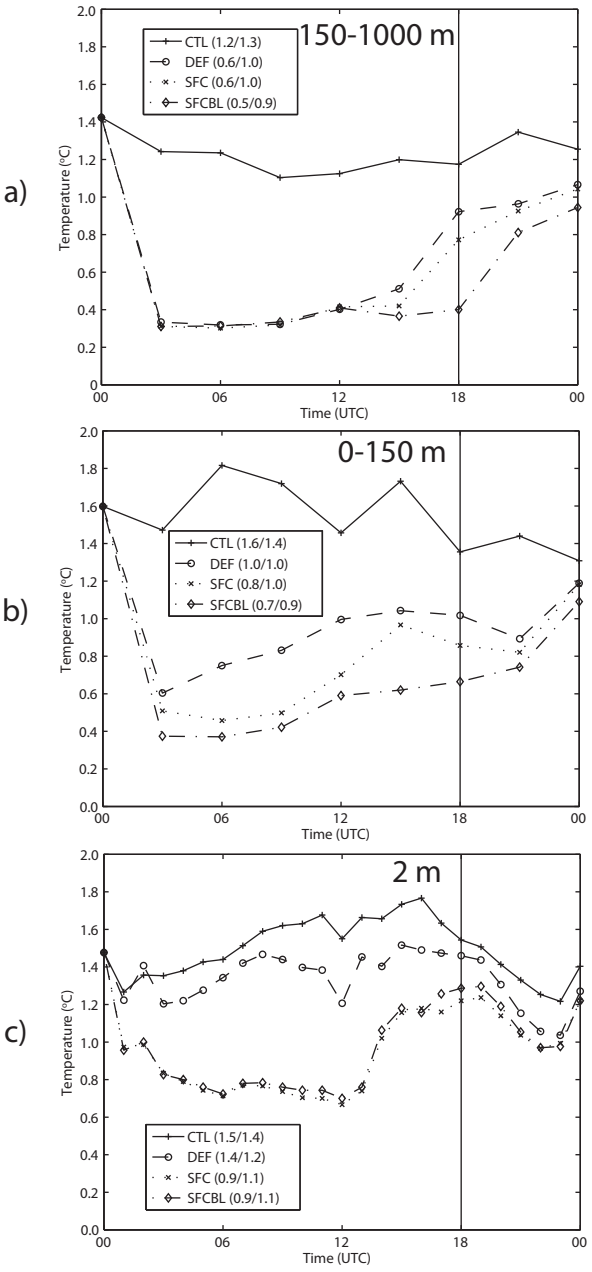

Fig. 5. Time series of domain-averaged air temperature MAE over the three case days at a) 150-1000 m, b) 0-150 m, and c) 2 m. The vertical line at 1800 UTC shows the end time of the pre-forecast data assimilation. The average for the pre-forecast period (0000-1800 UTC) and the average for the forecast period (1900-0000 UTC) calculated by weighting equally each time plotted are shown in the legend for each line.

surface observations to nudge atmospheric air temperature tended to alter the vertical temperature profile from the soil to the lower atmosphere, so Noah soil temperature was also nudged to decrease this problem and improve model air temperature predictions.

The assimilation of surface observations only can change the stabilization and degrade the PBL height. However, the addition of above-PBL observations removes this degradation. The use of within-PBL observations further reduces error throughout the PBL.

These results suggest that mass-field data properly assimilated at the surface and within the PBL can have significant positive impact in the boundary layer without disrupting the PBL height fields critically important for air chemistry and atmospheric transport and dispersion. The boundary layer data assimilation techniques tested here were effective for both a TKE scheme (GS) and a first-order scheme (MRF, not shown; Hong and Pan 1996; Liu et al. 2006) with each coupled to the Noah LSM. Since the WRF model also contains the Noah LSM and has both a TKE scheme (Mellor-Yamada-Janjic; Janjic 2002) and an updated version of the non-local first-order MRF scheme known as the Yonsei University scheme (YSU; Skamarock et al. 2005), the nudging techniques demonstrated here should be applicable to both MM5 and WRF.

Table 3. Model-diagnosed PBL height from 4-km 3D MM5 experiments compared to lidar-derived PBL height from aircraft transects for all transects in the 6-h forecast period.

Date	Exp.	PBL Height (m)		
		Mean	ME	MAE
29 May	CTL	1447	+156	327
	DEF	1392	+102	277
	SFC	1360	+69	273
	SFCBL	1345	+54	273
6 June	CTL	1406	+34	185
	DEF	1307	-65	167
	SFC	1276	-96	173
	SFCBL	1298	-74	172
7 June	CTL	1224	-380	407
	DEF	1403	-201	313
	SFC	1389	-216	320
	SFCBL	1384	-221	333
Mean	CTL	1359	-63	306
	DEF	1367	-55	252
	SFC	1342	-81	255
	SFCBL	1342	-80	259

7. ACKNOWLEDGMENTS

Steve Hanna is acknowledged for his expert manual diagnosis of PBL depth from the radiosonde data, Fei Chen and Kevin Manning for their provision of HRLDAS output, and Ricardo Muñoz for the 1D Matlab GUI version of MM5. Cyrille Flamant and colleagues are acknowledged for provision of Leandre II lidar data, Gerhard Ehret and colleagues for DLR DIAL lidar data, and Ken Craig for lidar-derived PBL height. This research was supported by DTRA W911NF-06-1-0439 under the supervision of John Hannan.

8. REFERENCES

Alapaty, Kiran, Devdutta Niyogi, and Madhavi Alapaty, 2001: An inverse technique for assimilating/adjusting soil moisture in the MM5. Preprints, *Eleventh PSU/NCAR MM5 Users' Workshop*, Foothills Laboratory, NCAR, June 25 – June 27, 2001.

Alapaty, K., D. Niyogi, F. Chen, P. Pyle, A. Chandrasekar, and N. Seaman, 2008: Development of the flux-adjusting surface data assimilation system for mesoscale models. *J. Appl. Meteor. Climatol.*.

Belair, S., L.-P. Crevier, J. Mailhot, B. Bilodeau, and Y. Delage, 2003: Operational implementation of the ISBA land surface scheme in the Canadian regional weather forecast model. Part I: Warm season results. *J. Hydrometeor.*, **4**, 352-370.

Benjamin, S. G., and N. L. Seaman, 1985: A simple scheme for objective analyses in curved flow. *Mon. Wea. Rev.*, **113**, 1184-1198.

Benjamin, S. G., S. S. Weygandt, D. Devenyi, J. M. Brown, G. Manikin, T. L. Smith, and T. G. Smirnova, 2004: Improved moisture and PBL initialization in the RUC using METAR data. Preprints, *22nd Conf. on Severe Local Storms*, Hyannis, MA, Amer. Meteor. Soc., 17.3.

Bruneau, D., P. Quaglia, C. Flamant, M. Meissonnier, and J. Pelon, 2001: Airborne lidar LEANDRE II for water-vapor profiling in the troposphere. *Appl. Opt.*, **40**, 3450-3475.

Chen, Fei, Kenneth Mitchell, John Schaake, Yongkang Xue, Hua-Lu Pan, Victor Koren, Qing Yun Duan, Michael Ek, and Alan Betts, 1996: Modeling of land surface evaporation by four schemes and comparison with FIFE observations. *J. Geophys. Res.*, **101**, D3, 7521-7268.

Chen, F., and Dudhia J., 2001: Coupling an advanced land surface—hydrology model with the Penn State—NCAR MM5 modeling system. Part I: Model implementation and sensitivity. *Mon. Wea. Rev.,* **129**, 569-585.

Chen, F., K. W. Manning, D. N. Yates, M. A. LeMone, S. B. Trier, R Cuenca, and D. Niyogi, 2004: Development of high resolution land data assimilation system and its application to WRF. Preprints. *20th Conf. on Weather Analysis and Forecasting/16th Conf. on Numerical Weather Prediction*, Seattle, WA, Amer. Meteor. Soc., 22.3.

Chen, F., K. W. Manning, M. A. LeMone, S. B. Trier, J. G. Alfieri, R. Roberts, M. Tewari, D. Niyogi, T. W. Horst, S. P. Oncley, J. B. Basara, and P. D. Blanken, 2007: Description and evaluation of the characteristics of the NCAR High-Resolution Land Data Assimilation System. *J. Appl. Meteor. Climatol.*, **46**, 694-713.

Childs, Peter P., Aneela L Qureshi, Sethu Raman, Kiran Alapaty, Robb Ellis, Ryan Boyles, and Dev Niyogi, 2006: Simulation of convective initiation during IHOP_2002 using the Flux-Adjusting Surface Data Assimilation System (FASDAS). *Mon. Wea. Rev.*, **134**, 134-148.

Coiffier, J., Y. Ernie, J.-F. Geleyn, J. Clochard, J. Hoffman, and F. Dupont, 1986: The operational hemispheric model at the French meteorological service. *Collection of Papers Presented at the WMO/IUGG NWP Symposium*, Tokyo, 4-8 August 1986. 337-345.

Deardorff, J. W., 1978: Efficient prediction of ground surface temperature and moisture, with inclusion of a layer of vegetation. *J. Geophys. Res.*, **83**, 1889-1903.

Dudhia, J., 1993: A nonhydrostatic version of the Penn State—NCAR Mesoscale Model: Validation tests and simulation of an Atlantic cyclone and cold front, *Mon. Wea. Rev.*, **121**, 1493-1513.

Ek, M. B., K. E. Mitchell, Y. Lin, E. Rogers, P. Grunman, V. Koren, G. Gayno, and J. D. Tarpley, 2003: Implementation of Noah land surface model advances in the National Centers for Environmental Prediction operational mesoscale Eta model. *J. Geophys. Res.*, **108**, 8851.

Gallus Jr., William A., and Moti Segal, 2001: Impact of improved initialization of mesoscale features on convective system rainfall in 10-km Eta simulations. *Wea. Forecasting*, **16**, 680-696.

Giard, D., and E. Bazile, 2000: Implementation of a new assimilation scheme for soil and surface variables in a global NWP model. *Mon. Wea. Rev.*, **128**, 997-1015.

Grell, G. A., J. Dudhia, and D. R. Stauffer, 1995: A description of the fifth-generation Penn State / NCAR Mesoscale Model (MM5), NCAR Tech. Note NCAR/TN-398+STR, 122 pp.

Hacker, J. P., and D. Roskier-Edelstein, 2007: PBL state estimation with surface observations, a column model, and an ensemble filter. *Mon. Wea. Rev.*, **135**, 2958-2972.

Hong, S.-Y., and H.-L. Pan, 1996: Nonlocal boundary layer vertical diffusion in a medium-range forecast model. *Mon. Wea. Rev.*, **124**, 2322-2339.

Janjic, Z. I., 2002: Nonsingular implementation of the Mellor-Yamada Level 2.5 Scheme in the NCEP Meso Model, *NCEP Office Note*, **No. 437**, 61 pp.

LeMone, M. A., F. Chen, J. G. Alfieri, R. H. Cuenca, Y. Hagimoto, P. Blanken, D. Niyogi, S. Kang, K. Davis, and R. L. Grossman, 2007: NCAR/CU surface, soil, and vegetation observations during the International H2O Project 2002 field campaign. *Bull. Amer. Meteor. Soc.*, **88**, 65-81.

Liu, Y., A. Bourgeois, T. Warner, S. Swerdlin, and J. Hacker, 2005: Implementation of observation-nudging based FDDA into WRF for supporting ATEC test operations. Preprints, *6th WRF / 15th MM5 Users' Workshop*, Boulder, CO, NCAR, 10.7. [Available online at http://www.mmm.ucar.edu/wrf/users/workshops/WS2005/WorkshopPapers.htm]

Liu, Yubao, Fei Chen, Thomas Warner, and Jeffrey Basara, 2006: Verification of a mesoscale data-assimilation and forecasting system for the Oklahoma City area during the Joint Urban 2003 field project. *J. Appl. Meteor. Climatol.*, **45**, 912-929.

Mlawer, E. J., S. J. Taubman, P. D. Brown, M. J. Iacono, and S. A. Clough, 1997: Radiative transfer for inhomogeneous atmospheres: RRTM, a validated

correlated-k model for the longwave. *J. Geophys. Res.*, **102** (D14), 16663-16682.

Pleim, J. E., and A. Xiu, 2003: Development of a land surface model. Part II: Data assimilation. *J. Appl. Meteor.*, **42**, 1811-1822.

Poberaj, G., A. Fix, A. Assion, M. Wirth, C. Kiemle, and G. Ehret, 2002: Airborne all-solid-state DIAL for water vapor measurements in the tropopause region: system description and assessment of accuracy. *Appl. Phys.*, **B75**, 165-172.

Reen, B. P. and D. R. Stauffer: Submitted: Data assimilation strategies and land-surface heterogeneity effects in the planetary boundary layer. Part I: 1D data assimilation experiments. Submitted to Mon. Wea. Rev.

Ruggiero, F. H., K. D. Sashegyi, R. V. Madala, and S. Raman, 1996: The use of surface observations in four-dimensional data assimilation using a mesoscale model. *Mon. Wea. Rev.*, **124**, 1018-1033.

Ruggiero, F. H., G. D. Modica, and A. E. Lipton, 2000: Assimilation of satellite imager data and surface observations to improve analysis of circulations forced by cloud shading contrasts. *Mon. Wea. Rev.*, **128**, 434-448.

Schroeder, A. J., D. R. Stauffer, N. L. Seaman, A. Deng, A. M. Gibbs, G. K. Hunter, and G. S. Young, 2006: An automated high-resolution, rapidly relocatable meteorological nowcasting and prediction system. *Mon. Wea. Rev.*, **134**, 1237-1265.

Seaman, N. L., D. R. Stauffer, and A. M. Lario-Gibbs, 1995: A multiscale four-dimensional data assimilation system applied in the San Joaquin Valley during SARMAP. Part I: Modeling design and basic performance characteristics. *J. Appl. Meteor.*, **34**, 1739-1761.

Shafran, P. C., N. L. Seaman, and G. A. Gayno, 2000: Evaluation of numerical predictions of boundary layer structure during the Lake Michigan Ozone Study. *J. Appl. Meteor.*, **39**, 412-426.

Skamarock, W. C., 2004: Evaluating mesoscale NWP models using kinetic energy spectra. *Mon. Wea. Rev.*, **132**, 3019-3032.

Stauffer, D. R., N. L. Seaman, and F. S. Binkowski, 1991: Use of four-dimensional data assimilation in a limited-area mesoscale model. Part II: Effects of data assimilation within the planetary boundary layer. *Mon. Wea. Rev.*, **119**, 734-754.

Stauffer, D. R., and N. L. Seaman, 1994: Multiscale four-dimensional data assimilation. *J. Appl. Meteor.*, **33**, 416-434.

Stauffer, David R., 1995: Multi-scale dynamic analysis of meteorology in complex terrain for air-quality applications. *7th Conference on Mountain Meteorology*, Breckenridge, CO, July 17 – July 21, 1995.

Weckwerth, T. M., D. B. Parsons, S. E. Koch, J. A. Moore, M. A. LeMone, B. B. Demoz, C. Flamant, B. Geerts, J. Wang, and W. F. Feltz, 2004: An overview of the International H2O Project (IHOP_2002) and some preliminary highlights. *Bull. Amer. Meteor. Soc.*, **85**, 253-277.

Zhang, Dalin, and Richard A. Anthes, 1982: A high-resolution model of the planetary boundary layer—sensitivity tests and comparisons with SESAME-79 data. *J. Appl. Meteor.*, **21**, 1594-1607.